Applied Surface Science 255 (2009) 8153–8157

Contents lists available at ScienceDirect

Applied Surface Science

journal homepage: www.elsevier.com/locate/apsusc

Ice adhesion on super-hydrophobic surfaces

S.A. Kulinich *, M. Farzaneh

CIGELE/INGIVRE, Department of Applied Sciences, University of Québec, 555, University Blvd., Saguenay, PQ G7H 2B1, Canada

ARTICLE INFO

Article history:
Received 22 August 2008
Received in revised form 6 May 2009
Accepted 18 May 2009
Available online 22 May 2009

PACS:
68.35.Md
68.08.Bc
82.45.Mp

Keywords:
Hydrophobicity
Ice adhesion
Shear stress
Contact angle hysteresis

ABSTRACT

In this study, ice adhesion strength on flat hydrophobic and rough super-hydrophobic coatings with similar surface chemistry (based on same fluoropolymer) is compared. Glaze ice, similar to naturally accreted, was prepared on the surfaces by spraying super-cooled water microdroplets at subzero temperature. Ice adhesion was evaluated by spinning the samples at constantly increasing speed until ice delamination occurred. Super-hydrophobic surfaces with different contact angle hysteresis were tested, clearly showing that the latter, along with the contact angle, also influences the ice–solid adhesion strength.

1. Introduction

Ice and wet-snow adhesion to outdoor surfaces is known to cause serious problems for power transmission lines, aircrafts, boats, etc. [1]. Even though there is no material to completely prevent ice/snow accretion on its surface [1–3], some coatings are believed to provide reduced adhesion. This is expected to result in lower ice and/or wet-snow accumulation on such surfaces [1,4,5]. Therefore, the research on coatings reducing frost, wet-snow and/or ice accumulation has been continuing for several decades [1–18].

Good correlation between hydrophobicity of surfaces and their ice-phobic behaviour was previously reported by several groups [7,15]. It was, however, disputed by others [6], who reported the absence of any correlation between the ice adhesion data and the contact angle (CA) on surface of plastics. Super-hydrophobic surfaces (i.e. those exhibiting water CA $> 150^{\circ}$) were tested by Saito et al. and demonstrated promising anti-icing performance [7], however, no systematic work on ice-repellent super-hydrophobic surfaces has been reported since then.

Several methods have been previously proposed to evaluate ice–solid adhesion [2,3,6,7,15,17–19]. In most cases, however, water was artificially frozen on top of samples tested, which is far from real icing conditions outdoors [3,6,7,15,17–19]. Therefore, testing adhesion of glaze ice prepared by spraying super-cooled water droplets is expected to give more reliable results [5]. In this work, we prepared glaze ice by spraying water microdroplets at subzero temperature, i.e. conditions very close to outdoor ice accretion. Ice adhesion was tested on polished aluminium and both flat and rough fluoropolymer-based samples with similar surface chemistry. Super-hydrophobic surfaces with different contact angle hysteresis (CAH) were tested, clearly showing that the latter, along with the contact angle, also influences the ice–solid adhesion strength.

2. Experimental procedures

Both flat (samples 1 and 2) and rough (3–6) samples were prepared in this study (see Table 1). AA6061 aluminium alloy plates, 3.2 cm × 5.0 cm in size, were used as substrates. Prior to coating, they were polished with emery paper and cleaned in organic solvents. The coating procedure was mainly adopted after Refs. [20–22] and is presented schematically in Fig. 1. Sample 1 was a bare (polished) plate of Al used as the standard, whereas sample 2 was a similar plate coated with fluoropolymer. ZrO_2 nanopowder from Aldrich was used for rough samples 3 and 4, while Ag nanoparticles prepared following Refs. [23] and [24,25] were used for samples 5 and 6, respectively. The powder or centrifugated particles (7.0 g in each case) were mixed with 80 ml of deionized water. The suspensions were sonicated for 30 min, after which 6.0 ml of Zonyl 8740 (a perfluoroalkyl methacrylic copolymer

* Corresponding author.
E-mail address: s_kulinich@yahoo.com (S.A. Kulinich).

0169-4332/$ – see front matter.
doi:10.1016/j.apsusc.2009.05.033

Table 1
Sample description and properties.

Sample	Nanoparticles used	CA (°)	CAH (°)	R_a (nm)	Description
1	–	57.3 ± 2.8	~50	6.2	Bare Al
2	–	120.1 ± 2.3	~40	3.9	Flat fluoropolymer
3	ZrO_2/20–30 nm	151.1 ± 2.4	>70	192	Sprayed
4	ZrO_2/20–30 nm	152.2 ± 1.5	7.8 ± 2.2	229	Spin-coated
5	Ag/80–400 nm	153.3 ± 1.3	8.1 ± 1.8	249	Spin-coated
6	Ag/100–600 nm	151.5 ± 1.4	9.5 ± 1.7	242	Spin-coated

product from DuPont [20–22]) were added. The final suspensions were stirred for another 3 h before coating the substrates. Super-hydrophobic sample 3 was prepared by spraying the ZrO_2 suspension over the substrate surface uniformly and letting it dry at ~50 °C [22]. The nozzle of a commercially available manual sprayer was kept at ~10 cm from the substrate, and the suspension was sprayed until the surface was fully covered with a liquid layer. Super-hydrophobic samples 4–6 were prepared by spin-coating of corresponding suspensions on the substrate. The spinning speed was set at 200 rpm (5 s) and 3000 rpm (10 s) for the first and second steps, respectively. More detailed description of the samples and their characteristics are given in Table 1. Use of different nanoparticles and spray or spin-coating allowed to prepare samples with different surface topographies and wetting hysteresis, as discussed below. Hydrophobic sample 2 was prepared similar to sample 3 except for no nanoparticles were used, which led to a flat surface. Upon coating, all samples were heat-treated at 120 °C in air for 3 h to remove residual solvents.

Both CA and CAH values were measured on a Krüss DSA10 contact-angle goniometer following standard procedures. Contact angles were measured by the sessile-drop method; small water droplets were gently placed on the surface, and their shape was evaluated by using the goniometer optics and software. The values reported herein were the average of at least five measurements on various parts of each sample. They were recorded at 23 ± 0.5 °C with distilled water; all droplets were 4 μl in volume. For advancing CAs, a small drop was deposited on the surface, and then additional water was added to advance the contact line. For receding CAs, water was withdrawn until the contact line retracted. Measurements were made on both sides of more than five droplets and then averaged.

Scanning electron microscopy (SEM) of the sample surfaces was carried out with a JSM-6330-F microscope (JEOL) after covering them with a thin conducting layer of Pt. Surface topographies were

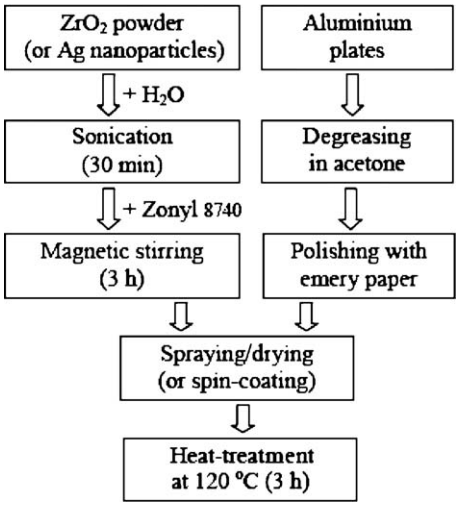

Fig. 1. Schematic representation of coating procedure.

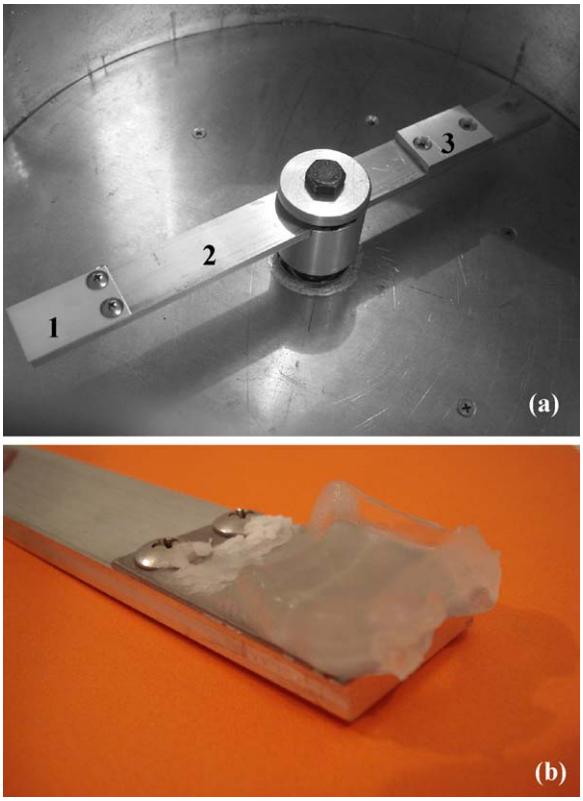

Fig. 2. (a) Coated sample in centrifuge set-up measuring ice adhesion: (1) sample, (2) Al beam and (3) counter-weight. (b) Sample with artificial glaze ice.

also analyzed with a WYKO NT1100 optical profilometer (Veeco). X-ray photoelectron spectroscopy (XPS) was performed with a Quantum-2000 instrument from ULVAC-PHI.

The ice-adhesion evaluation tests were conducted on Al beams with samples spun in a centrifuge (see Fig. 2a). The samples attached to the beams were iced in a wind tunnel at a wind speed of 10 m/s, temperature −10 °C, water feed rate of 2.5 g/m^3 and average droplet size of ~80 μm to prepare glaze ice of up to ~1 cm thick over the area of ~3.2 cm × 3.0 cm (Fig. 2b). This ice geometry was enough to avoid cohesion failure and provide reproducible results during deicing. Ice mass and area were carefully evaluated both after icing and deicing. To balance the beam in the centrifuge, a counter-weight was used on the other side (see Fig. 2a). The artificially iced samples were then spun in the centrifuge placed in a climatic chamber at −10 °C to determine the speed at which ice detachment from the sample surface occurs. At the moment of the detachment (detected with sensors embedded into the centrifuge walls), the adhesion strength of ice was assumed to be equal to the centrifugal force, $F = mr\omega^2$, where m is the ice mass, r is the beam radius and ω is the rotation speed in rad/s. The shear stress, correspondingly, was calculated as $\tau = F/A$, where A is the deiced area. To reduce the influence of any experimental errors, the adhesion reduction factor, *ARF*, was finally used rather than absolute values of shear stress. *ARF* was calculated as the ratio of ice shear stress on bare polished Al (sample 1) to that on samples with coatings, $ARF = \tau_{(Al)}/\tau_{(coating)}$, provided that all the tests were run for both uncoated and coated samples under identical conditions. Three pieces were prepared for each sample in Table 1, and the results were calculated as the average of the three.

3. Results and discussion

Only F, Zr (or Ag), C, O and Al peaks were observed in XPS survey spectra of all super-hydrophobic samples 3–6 (not shown here).

The presence of the Al signal implies some porosity of the coatings, which is in agreement with their surface images in Figs. 3 and 4. Surface composition of samples 3 and 4, calculated from their XPS spectra, was very similar. Furthermore, samples 5 and 6 also demonstrated very similar XPS spectra, except for Ag signals were detected instead of those of Zr. In combination with the high values of CA observed for samples 3–6 (see Table 1), this implies that all nanoparticles are well covered with fluoropolymer and thus all the samples have very similar surface chemistry. This conclusion is in good agreement with the previously published reports by others [20–22]. An XPS spectrum of the flat sample 2 was very similar to those of the rough samples but did not demonstrate any Zr, Ag or Al signals, implying complete coverage of the substrate with fluoropolymer.

Table 1 presents surface roughness (R_a) and wetting characteristics of the samples used in this study. Surface images of rough super-hydrophobic samples are shown in Figs. 3 and 4, while Fig. 5 presents surface profiles of the flat sample 2 and rough samples 3 and 4. Fig. 3 compares samples 3(a) and 4(b) prepared from the same ZrO_2 suspension by means of spraying (Fig. 3a) or spin-coating (Fig. 3b) and demonstrating contrasting CAH (see Table 1 and insets in Fig. 3). Both surfaces are seen to be rough at microscale. Their roughness, R_a, measured by profilometry over

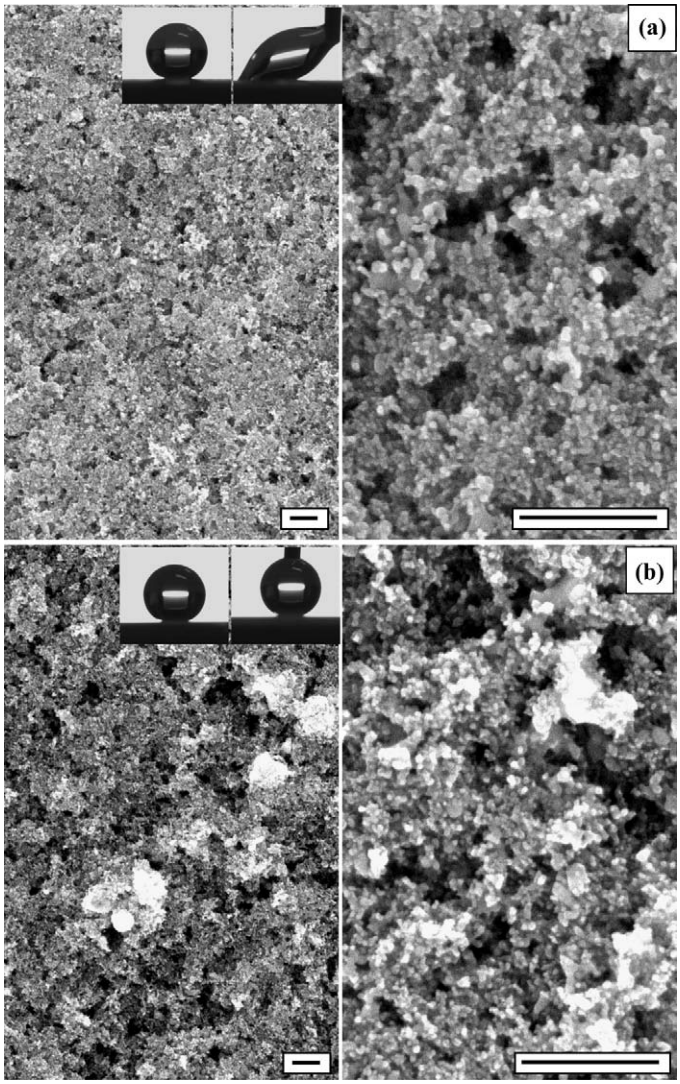

Fig. 3. Surface images of samples 3(a) and 4(b) prepared from ZrO_2 nanopowder. Sessile and moving water droplets are shown as insets. Scale bars indicate 500 nm.

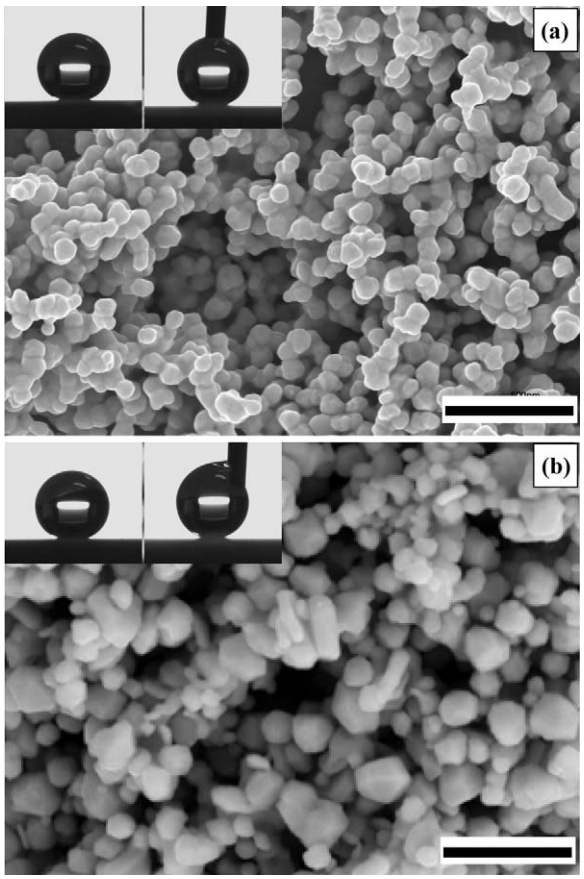

Fig. 4. SEM images of samples 5(a) and 6(b) prepared from Ag nanoparticles. Sessile and moving water droplets are shown as insets. Scale bars indicate 1 μm.

areas of 59 μm × 45 μm was evaluated as 192 and 229 nm for samples 3 and 4, respectively. Thus air entrapment into their structure is expected during wetting. However, the surface asperities in Fig. 3a are less separated and have relatively flat and shallow tops, whereas the asperities in Fig. 3b appear to be sharper and better spaced. This is also well seen in Fig. 5b and c where surface profiles for samples 3 and 4 are compared; note better separated and taller asperities in Fig. 5c and less separated asperities with shallow tops in Fig. 5b. Therefore, while the Cassie–Baxter wetting mode is expected on sample 4, a mixed (Cassie–Baxter and Wenzel) mode is likely on sample 3 [4,22,26]. As a result, the water–solid contact area on sample 3 is expected to be larger than that on sample 4, which is in agreement with the contrasting wetting hysteresis observed on these samples (see insets in Fig. 3a and b).

Surface images of samples 5 and 6 prepared from Ag nanoparticles with different size are presented in Fig. 4a and b, respectively. In both cases, rough surfaces are observed, implying air entrapment into the structures when water droplet is placed atop. As surface asperities are well separated in both images in Fig. 4, high CA and "slippy" surface state [4,22,26–29] can be expected for water drops on both samples, which is consistent with the insets in Fig. 4a and b.

As in nature icing events occur under more dynamic conditions than those previously applied to test ice adhesion on materials [3,6,7,15,17–19], this implies the dynamic hydrophobicity of surfaces may play some role. This assumption is in agreement with those previous reports where various dynamic aspects of surface hydrophobicity (in addition to CA) were proposed to be taken into account to characterize surface water repellency [4,11,14,27–31]. Therefore, to test the influence of the dynamic

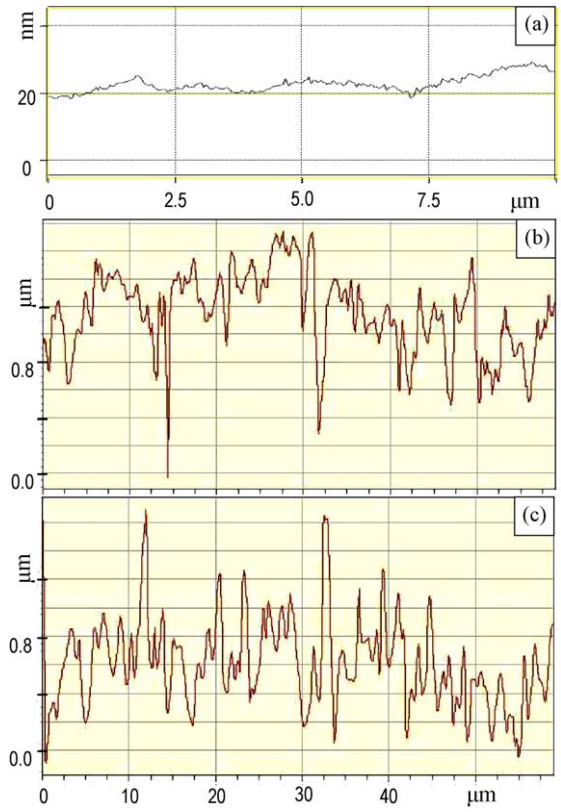

Fig. 5. Surface profiles of samples 2(a), 3(b) and 4(c).

hydrophobicity of the surface on icing/deicing, rough samples with contrasting wetting hysteresis were prepared (compare sample 3 and samples 4–6 in Table 1).

Fig. 6a presents *ARF* values obtained for all the samples in Table 1. The results obtained on the uncoated Al and flat fluoropolymer-coated samples (1 and 2 in Fig. 6a) are consistent

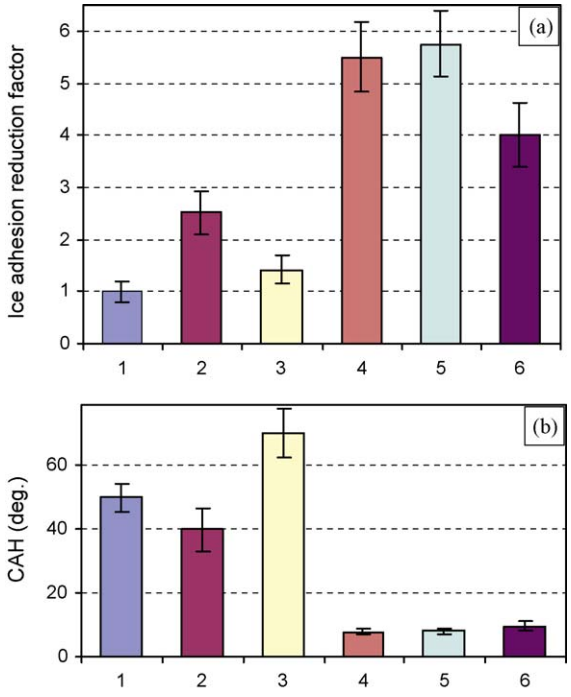

Fig. 6. Values of ice adhesion reduction factor (*ARF*) (a) and contact angle hysteresis (b) for samples used. Sample numbers correspond to Table 1.

with those of Somlo and Gupta [17], who reported ~1.4–2.1 times lower ice adhesion on organosilane-coated AA6061 when compared to bare AA6061 with various surface finish. It is seen that ice adhesion on the flat fluoropolymer (sample 2) is ~2.5 times lower than that on the bare polished aluminium (sample 1). This is also in agreement with the general belief that low-energy surfaces demonstrate reduced ice adhesion [2,4,13–15].

The adhesion strength of ice on the high-hysteresis sample 3 is seen in Fig. 6a to be surprisingly high, if compared to the other super-hydrophobic samples, and quite close to that on the uncoated sample 1. Samples 4–6 demonstrate their *ARF* values within the range of ~4–5.7, implying ice adhesion strength on the low-hysteresis super-hydrophobic surfaces a few times lower than on the flat fluoropolymer sample 2. Also, instead of a direct correlation between the surface CA and decreased ice adhesion strength, previously reported for both flat [15] and rough [7] surfaces, the ice adhesion on rough samples 3–6 is seen to correlate with their CAH (see Fig. 6a and b). This is believed to result from different ice–solid contact areas on rough surfaces, which are realized on the rough samples with different values of CAH. Such contact areas are expected to be inherited mainly from the initial water–solid contact areas during icing, and the water–solid contact area on rough surfaces with similar surface chemistry is expected to be directly related to their CAH [22,26]. This correlation between the ice adhesion strength on super-hydrophobic surfaces and their CAH was not observed in the previous work of Saito et al. [7] since all their samples appeared to have low CAH values and ice was prepared by simply freezing water on top of the samples. Under such conditions, the ice–solid contact area is expected to decrease with increase in CA. This explains well why the Teflon-based samples in work [7] demonstrated ice repellency improving with increased CA values, which is also the case for the low-CAH super-hydrophobic surfaces (samples 4–6) observed in this study. As in the present work we tested samples with contrasting CAH, the influence of the CAH on the ice adhesion strength on rough super-hydrophobic surfaces was found.

4. Summary

Adhesion of ice, prepared from super-cooled water droplets and thus similar to that accreted on outdoor structures, has been measured on hydrophobic and super-hydrophobic coatings with similar chemical composition and compared to that on uncoated polished aluminium. On super-hydrophobic surfaces observed in this study, ice adhesion correlates rather with wetting hysteresis of the surfaces, being lower on low-hysteresis surfaces. This can be explained by the larger water–solid (and thus ice–solid) area that is expected for the high-hysteresis sample. On super-hydrophobic surfaces with low wetting hysteresis, ice adhesion strength was observed to be up to ~5.7 times lower than on bare polished aluminium.

Acknowledgments

This work was supported by Hydro-Québec, Hydro One, Alcan Cable, K-Line Insulators, CQRDA, and FUQAC. The authors also thank Dr. K. Nose (Univ. Tokyo) and Dr. A. Safaee (Univ. Quebec) for their assistance with analyses.

References

[1] J.L. Laforte, M.A. Allaire, J. Laflamme, Atmos. Res. 46 (1998) 143–158.
[2] V.K. Croutch, R.A. Hartley, J. Coat. Technol. 64 (1992) 41–52.
[3] L.O. Andersson, C.G. Golander, S. Persson, J. Adhes. Sci. Technol. 8 (1994) 117–132.
[4] S.A. Kulinich, M. Farzaneh, Surf. Sci. 573 (2004) 379–390.
[5] R. Menini, M. Farzaneh, Surf. Coat. Technol. 203 (2009) 1941–1946.
[6] M. Landy, A. Freiberger, J. Colloid Interface Sci. 25 (1967) 231–244.

[7] H. Saito, K. Takai, G. Yamauchi, Surf. Coat. Int. 80 (1997) 168–171.
[8] H. Murase, K. Nanishi, H. Kogure, T. Fujibayashi, K. Tamura, N. Haruta, J. Appl. Polym. Sci. 54 (1994) 2051–2062.
[9] T. Kako, A. Nakajima, Z. Kato, K. Uematsu, T. Watanabe, K. Hashimoto, J. Ceram. Soc. Jpn. 110 (2002) 186–192 (in Japanese).
[10] S.A. Kulinich, M. Farzaneh, Appl. Surf. Sci. 230 (2004) 232–240.
[11] A. Nakajima, J. Ceram. Soc. Jpn. 112 (2004) 533–540.
[12] T. Kako, A. Nakajima, H. Irie, Z. Kato, K. Uematsu, T. Watanabe, K. Hashimoto, J. Mater. Sci. 39 (2004) 547–555.
[13] M. Futamata, X. Gai, H. Itoh, Vacuum 73 (2004) 519–525.
[14] S.A. Kulinich, M. Farzaneh, Vacuum 79 (2005) 255–264.
[15] V.F. Petrenko, S. Peng, Can. J. Phys. 81 (2003) 387–393.
[16] H. Wang, L.M. Tang, X.M. Wu, W.T. Dai, Y.P. Qiu, Appl. Surf. Sci. 253 (2007) 8818–8824.
[17] B. Somlo, V. Gupta, Mech. Mater. 33 (2001) 471–480.
[18] L.E. Raraty, D. Tabor, Proc. R. Soc. Lond., Ser. A 245 (1958) 184–201.
[19] H.H.G. Jellinek, Can. J. Phys. 40 (1962) 1294–1309.
[20] H.-I. Hsiang, M.-T. Liang, H.-C. Huang, F.-S. Yen, Mater. Res. Bull. 42 (2007) 420–427.
[21] T.-Y. Han, J.-F. Shr, C.-F. Wun, C.-T. Hsieh, Thin Solid Films 515 (2007) 4666–4669.
[22] S.A. Kulinich, M. Farzaneh, Appl. Surf. Sci. 255 (2009) 4056–4060.
[23] M. Andersson, J.S. Pedersen, A.E.C. Palmqvist, Langmuir 21 (2005) 11387–11396.
[24] Y. Sun, Y. Xia, Science 298 (2002) 2176–2179.
[25] D. Kim, S. Jeong, J. Moon, Nanotechnology 17 (2006) 4019–4024.
[26] A. Nakajima, K. Hashimoto, T. Watanabe, Monatsh. Chem. 132 (2001) 31–41.
[27] D. Öner, T.J. McCarthy, Langmuir 16 (2000) 7777–7782.
[28] R. Rioboo, M. Voué, A. Vaillant, J. De Coninck, Langmuir 24 (2008) 14074–14077.
[29] W. Chen, A.Y. Fadeev, M.C. Hsieh, D. Öner, J. Youngblood, T.J. McCarthy, Langmuir 15 (1999) 3395–3399.
[30] S. Suzuki, A. Nakajima, M. Sakai, J.-H. Song, N. Yoshida, Y. Kameshima, K. Okada, Surf. Sci. 600 (2006) 2214–2219.
[31] M. Sakai, J.-H. Song, N. Yoshida, S. Suzuki, Y. Kameshima, A. Nakajima, Surf. Sci. 600 (2006) L204–L208.